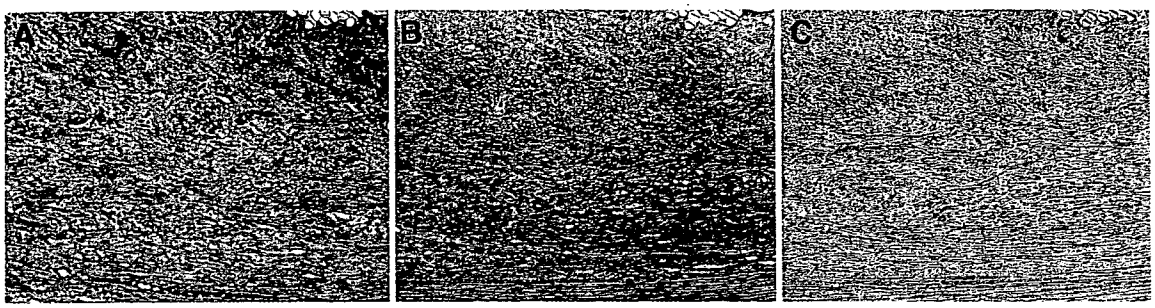

Figure 5 ◆ Histological cross sections of the neointimal tissue between the aortic wall and graft material in the bFGF group [hematoxylin-eosin (**A**), elastica van Gieson (**B**), α-SM actin stain (**C**); original magnification ×200]. The neointima consisted of fibrous tissue, inflammatory cells, collagen, and some elastin. These new tissues had large quantities of α-SM actin–positive cells.

between the aortic media and the graft, contained fibrous tissue, inflammatory cells, collagen, and a little elastin. In contrast, the inner spaces of the graft (luminal side) were occupied by more loose fibrous tissue, collagen, and elastin (Fig. 5). The neointima contained numerous α-SM actin–positive cells on both sides of the graft. These findings were observed in all groups. No capillary ingrowth was seen in any group.

Although the grafts were close-woven, new cells were observed infiltrating the spaces between the fibers of the graft, and the α-SM actin–positive cells were more abundant (Fig. 6), whereas fewer α-SM actin–positive cells were observed in the other groups. The total numbers of α-SM actin–positive cells within the graft materials per axial section were 99.5±35.4 in the control group, 133.5±34.3 in the hydrogel group, and 248.0±55.1 in the bFGF group. There were significant differences between the control and bFGF groups ($p<0.001$) and the hydrogel and bFGF groups ($p=0.001$).

The neointimal ratio was 9.3%±3.4% in the control group, 12.6%±4.2% in the hydrogel group, and 21.3±7.5% in the bFGF group. The differences in these ratios between the hydrogel and bFGF groups ($p=0.02$) and between the control and bFGF groups ($p=0.004$) were statistically significant. The intimal thickness was 11.3±7.7 μm in the control group, 19.7±10.9 μm in the hydrogel group, and 38.0±23.7 μm in the bFGF group ($p=0.026$ versus control).

DISCUSSION

Endovascular stent-grafting for aortic diseases is widely performed, but endoleaks

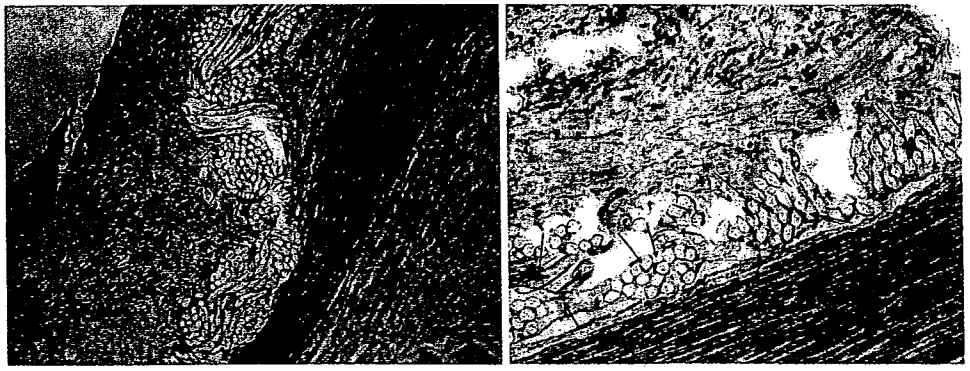

Figure 6 ◆ Histological cross sections in the bFGF group (α-SM actin staining, magnification ×100). New cells were observed between the fibers of the graft, and some α-SM actin–positive cells were also seen in the bFGF group (arrows).

and endotension are critically important problems of this procedure.[6–8] Since the goal of stent-grafting is not only prevention of aneurysmal growth but also shrinkage of the aneurysm, biological fixation of the graft to the aortic wall at the neck is important. However, polyester graft material, which is most widely used in aortic stent-grafts, does not fix to the vessel wall and does not heal adequately. Malina et al.[17] have shown that healing provides poor fixation of Dacron stent-grafts in humans, and fixation relies on the mechanical properties of the stent-grafts, which are exposed to high, pulsatile blood pressure. Unless there is firm perigraft healing between the graft and the aortic wall, biological fixation seems unlikely.

bFGF, a naturally occurring substance in human beings, was originally characterized in vitro as a growth factor for fibroblasts and capillary endothelial cells. In vivo, this growth factor plays an important role in the proliferation of a variety of cells, including mesodermal and neuroectodermal cells. In blood vessels, it has been demonstrated to stimulate the proliferation and migration of endothelial cells, SMCs, and fibroblasts.[18] However, the simple application of bFGF in a solution exerts no biological activity because of its short half-life in vivo, so the controlled release of bFGF is essential. Tabata et al.[14] developed a biodegradable gelatin hydrogel carrier for this purpose. Using this system, they confirmed that biologically active bFGF was released to the surrounding tissue gradually as a result of in vivo hydrogel degradation, whose rate is dependent on its water content.[14,16] Hence, it is possible to change the degradation time by adjusting the water content. In this study, we chose a 1-week degradation time because we wanted to see the reaction after bFGF release within a limited observation period.

In this study, we tested the hypothesis that the controlled release of bFGF from a stent-graft would accelerate aortic healing (including intimal hyperplasia), resulting in biological fixation with the aortic wall compared with a stent-graft without bFGF incorporation. To that purpose, we developed a new type of polyester-based stent-graft coated with hydrogels that allow controlled release of ~100 μg of bFGF over 1 week. All the materials used for this new device have been applied clinically.

Our results revealed that bFGF significantly accelerated the proliferation of new intimal tissue. However, accelerated proliferation was also seen in hydrogel-coated stent-grafts without bFGF, but the increase was minimal and not significantly different compared to the control group. We speculate that this could be due to the potential biocompatibility of the gelatin hydrogel, which itself could serve as a scaffold for cell proliferation. Therefore, the accelerated neointima formation seen in this study was mainly due to bFGF release and partially due to the biological reaction of hydrogel itself. In vivo, these cell proliferations presented as mild stenosis of the aorta. When applied to a small artery, this could be a concern, but it would not be clinically relevant in the large human aorta.

Since this was a preliminary study, the amount of bFGF employed was the maximal dose we could impregnate and the degradation time was short so as to estimate the initial reaction of the surrounding tissue. More investigations would be needed when the technique is applied to human beings.

Another important finding of the histological evaluation was the existence of α-SM actin–positive cells, probably SMCs or myofibroblasts, not only in new intimal tissue but also within the fabric of the tightly woven polyester graft. In cases of in-stent restenosis, Kearney et al.[19] reported that new tissue is composed of α-SM actin–positive cells with phenotypic characteristics of "activated" SMCs surrounded by a loose, light-staining extracellular matrix. The role of SMCs is to maintain the strength and elasticity of the aortic wall by producing elastin, collagen, and other matrix proteins.[20] In this study, the existence of α-SM–positive cells within the graft might represent the process of cell and matrix proliferation through the graft material.

According to these observations, we postulate that hyperplastic neointima occupying the space between the aortic wall and graft infiltrates into the spaces between the graft fibers, connecting with the neointima on the luminal side of the graft to achieve biological fixation of the stent-graft. This process can be

strongly enhanced by bFGF, which could make the biological fixation tighter and more durable, probably due to expected development of α-SM actin–positive cells.

van der Bas et al.[21] were the first to attempt to combine endovascular aortic aneurysm repair and bFGF. They showed that Dacron prostheses impregnated with collagen, heparin, and bFGF induced graft healing in vitro[21] and in a pig model[22] compared to non-impregnated stent-grafts. There are several differences between their work and our study, such as the porosity of the graft, the drug carrier, and the method of coating. In spite of these differences, we obtained similar results, demonstrating that stent-graft impregnation with bFGF was clearly beneficial for biological fixation with the aortic wall.

Limitations

First, the aortas used in this study had no atherosclerosis. Second, the observation period was relatively short. We surmised that increasingly more cell proliferation would occur as the observation period was prolonged, but we considered that 1 month was long enough to check initial reactions and predict possible changes of the aortic wall.

Third, we inserted 3 stent-grafts per pig to reduce the experimental period and costs; this design feature might have influenced the results. However, we deployed the stent-graft incorporated with bFGF in the most downstream portion of the aorta to avoid any secondary effect caused by released bFGF.

Fourth, there is a possibility that some injuries to the distal aorta might have occurred during implantation of the stent-grafts and thus have influenced to some degree the healing of the device, especially the more distally placed bFGF stent-grafts. However, because there was no difficulty or friction during insertion of the sheath catheter, it was considered to be unlikely that the distal aorta was injured.

Lastly, the real-time measurement of released bFGF in vivo was impossible technically in our study, but we assumed that hydrogel degradation and bFGF release to the surrounding aortic wall might be similar to previous studies.[14]

Conclusion

The local, controlled release of bFGF from the hydrogel coating on the surface of a polyester stent-graft significantly accelerated the proliferation of new intimal tissue on the aorta and within the graft in a porcine model. These findings suggest that the graft surface and aortic wall can be fixed biologically. It is highly likely that the tight attachment of a stent-graft and aortic neck may reduce minor type I endoleak or endotension. To evaluate the healing between the bFGF-coated stent-graft and an aortic aneurysm, further study using an aortic aneurysm model is required.

REFERENCES

1. Leurs LJ, Bell R, Degrieck Y, et al. Endovascular treatment of thoracic aortic diseases: combined experience from the EUROSTAR and United Kingdom Thoracic Endograft registries. *J Vasc Surg.* 2004;40:670–680.
2. Doss M, Wood JP, Balzer J, et al. Emergency endovascular interventions for acute thoracic aortic rupture: four-year follow-up. *J Thorac Cardiovasc Surg.* 2005;129:645–651.
3. Brandt M, Hussel K, Walluscheck KP, et al. Stent-graft repair versus open surgery for the descending aorta: a case-control study. *J Endovasc Ther.* 2004;11:535–538.
4. Greenhalgh RM, Brown LC, Kwong GP, et al. Comparison of endovascular aneurysm repair with open repair in patients with abdominal aortic aneurysm (EVAR trial 1), 30-day operative mortality results: randomised controlled trial. *Lancet.* 2004;364:843–848.
5. Prinssen M, Verhoeven EL, Buth J, et al. A randomized trial comparing conventional and endovascular repair of abdominal aortic aneurysms. *N Engl J Med.* 2004;351:1607–1618.
6. Veith FJ, Baum RA, Ohki T, et al. Nature and significance of endoleaks and endotension: summary of opinions expressed at an international conference. *J Vasc Surg.* 2002;35:1029–1038.
7. Gilling-Smith G, Brennan J, Harris P, et al. Endotension after endovascular aneurysm repair: definition, classification, and strategies for surveillance and intervention. *J Endovasc Surg.* 1999;6:305–307.
8. White GH, Yu W, May J, et al. Endoleak as a complication of endoluminal grafting of abdominal aortic aneurysms: classification, incidence, diagnosis, and management. *J Endovasc Surg.* 1997;4:152–168.

9. Marty B, Leu AJ, Mucciolo A, et al. Biologic fixation of polyester-versus polyurethane-covered stents in a porcine model. *J Vasc Interv Radiol.* 2002;13:601–607.
10. Szilagyi DE. The problem of healing of endovascular stent grafts in the repair of abdominal aortic aneurysms. *J Vasc Surg.* 2001;33: 1283–1285.
11. Asai J, Takenaka H, Ichihashi K, et al. Successful treatment of diabetic gangrene with topical application of a mixture of peripheral blood mononuclear cells and basic fibroblast growth factor. *J Dermatol.* 2006;33:349–352.
12. Akita S, Akino K, Imaizumi T, et al. A basic fibroblast growth factor improved the quality of skin grafting in burn patients. *Burns.* 2005; 31:855–858.
13. Conklin BS, Wu H, Lin PH, et al. Basic fibroblast growth factor coating and endothelial cell seeding of a decellularized heparin-coated vascular graft. *Artif Organs.* 2004;28:668–675.
14. Tabata Y, Nagano A, Ikada Y. Biodegradation of hydrogel carrier incorporating fibroblast growth factor. *Tissue Eng.* 1999;5:127–138.
15. Sanada J, Matsui O, Terayama N, et al. Clinical application of a curved nitinol stent-graft for thoracic aortic aneurysms. *J Endovasc Ther.* 2003;10:20–28.
16. Tabata Y, Ikada Y. Vascularization effect of basic fibroblast growth factor released from gelatin hydrogels with different biodegradabilities. *Biomaterials.* 1999;20:2169–2175.
17. Malina M, Brunkwall J, Ivancev K, et al. Endovascular healing is inadequate for fixation of Dacron stent-graft in human aortoiliac vessels. *Eur J Vasc Endovasc Surg.* 2001;19:5–11.
18. Slavin J. Fibroblast growth factors: at the heart of angiogenesis. *Cell Biol Int.* 1995;19:431–444.
19. Kearney M, Pieczek A, Haley L, et al. Histopathology of in-stent restenosis in patients with peripheral artery disease. *Circulation.* 1997;95: 1998–2002.
20. Bashar AH, Kazui T, Terada H, et al. Histological changes in canine aorta 1 year after stent-graft implantation: implications for the long-term stability of device anchoring zones. *J Endovasc Ther.* 2002;9:320–332.
21. van der Bas JM, Quax PH, van den Berg AC, et al. Ingrowth of aorta vascular cells into basic fibroblast growth factor-impregnated vascular prosthesis material: a porcine and human in vitro study on blood vessel prosthesis healing. *J Vasc Surg.* 2002;36:1237–1247.
22. van der Bas JM, Quax PH, van den Berg AC, et al. Ingrowth of aorta wall into stent grafts impregnated with basic fibroblast growth factor: a porcine in vivo study of blood vessel prosthesis healing. *J Vasc Surg.* 2004;39:850–858.

Eur Radiol (2007) 17: 2969–2982
DOI 10.1007/s00330-007-0705-z

Stavros C. Efremidis
Prodromos Hytiroglou
Osamu Matsui

Enhancement patterns and signal-intensity characteristics of small hepatocellular carcinoma in cirrhosis: pathologic basis and diagnostic challenges

Received: 14 December 2006
Revised: 31 May 2007
Accepted: 1 June 2007
Published online: 6 July 2007

S. C. Efremidis (✉)
Department of Radiology, University of Ioannina Medical School,
P.O. Box 1186, 45110 Ioannina, Greece
e-mail: sefremid@cc.uoi.gr
Tel.: +30-265-1097730
Fax: +30-265-1097862

P. Hytiroglou
Department of Pathology, Aristotle University of Thessaloniki Medical School,
54006 Thessaloniki, Greece

O. Matsui
Kanazawa University Graduate School of Medical Science,
13-1 Takara-machi,
Kanazawa, 920-8641, Japan

Abstract Recent pathologic studies of hepatic resection and transplantation specimens have elucidated the morphologic features of the precancerous lesions and small hepatocellular carcinomas (HCCs) arising in cirrhotic livers. Small HCCs measuring less than 2 cm in diameter are of two types: vaguely nodular, well-differentiated tumors, also known as "early" HCCs, and distinctly nodular tumors, with histologic features of "classic" HCC. The precancerous lesions include dysplastic foci and dysplastic nodules. "Classic" small HCCs are supplied by nontriadal arteries, whereas early HCCs and dysplastic nodules may receive blood supply from both portal tracts and nontriadal arteries. The similarities in blood supply of these three types of nodular lesions result in significant overlap of findings on dynamic imaging. Nevertheless, small HCCs sometimes display characteristic radiologic features, such as "nodule-in-nodule" configuration and "corona enhancement" pattern. Moreover, various histologic features of these nodular lesions may also be related to a variety of signal intensities and attenuation coefficients, while the presence of cirrhosis is known to limit the sensitivity and specificity of any imaging modality, due to liver inhomogeneity. Because of these reasons, imaging findings of nodular lesions in cirrhotic livers are often inconclusive, emphasizing the need for a better understanding of these imaging features.

Keywords Hepatocellular carcinoma · Nodular lesions · Magnetic resonance imaging · Computed tomography · Cirrhosis

Introduction

The great majority of hepatocellular carcinomas (HCCs) develop in patients with chronic liver disease, especially chronic viral hepatitis and cirrhosis. It is now well established that HCCs develop from precancerous (dysplastic) lesions, including dysplastic foci and dysplastic nodules [1]. On pathologic examination, such dysplastic lesions are almost always detected in cirrhotic livers; however, the evolution of the molecular changes leading to their formation often starts before cirrhosis is established [2]. In addition to defining the histologic features of dysplastic lesions, recent studies have better delineated the features of small HCCs, i.e., HCCs measuring less than 2 cm [3]. Small HCCs are of two types: vaguely nodular, well-differentiated lesions ("early" HCCs), and distinctly nodular lesions, histologically similar to larger HCCs (small HCCs of distinctly nodular type).

Computerized tomography (CT), magnetic resonance imaging (MRI) and ultrasound (US) have all been utilized for the evaluation of large liver nodules developing in cirrhosis. Different techniques of liver enhancement to distinguish benign from malignant nodules in the cirrhotic liver, such as dynamic multiphase CT or MRI, CT during hepatic arteriography (CTHA), and CT during arterial portography (CTAP) have been used with good results [4–7]. Contrast media with special physiologic properties and biodistribution have also been utilized in MRI to success-

fully address specific diagnostic problems in some cases [8, 9]. Recently, contrast media utilizing microbubbles as an enhancing agent have been developed for the sonographic characterization of focal liver lesions with high accuracy [10].

The aim of this review is to address the frequently encountered difficulties in differentiating among the various precancerous lesions and small HCCs arising in cirrhosis using MR signal intensity and CT attenuation characteristics before and after contrast administration. For this purpose, it is necessary (1) to describe the basic histologic features of the nodular lesions developing in cirrhosis and representing successive steps in the process of hepatocarcinogenesis, and (2) to correlate these features with imaging findings that are considered most typical for the characterization of small HCCs.

Basic pathologic features of dysplastic lesions and small hepatocellular carcinomas

Dysplastic lesions

The earliest lesions of the cirrhotic liver that are histologically detectable as being of precancerous nature are the dysplastic foci and the dysplastic nodules [1]. These lesions are often multiple, indicating that carcinogenesis in the cirrhotic liver is a multifocal process. By definition, dysplastic foci are minute lesions, measuring less than 0.1 cm in diameter; therefore, they are not demonstrable by imaging. Dysplastic nodules are larger than dysplastic foci and sometimes exceed 1.0 cm in greatest dimension. These lesions appear distinct from the surrounding regenerative nodules on gross pathologic examination and may be detected on radiologic examination, raising issues of differential diagnosis with large regenerative nodules and HCC.

Dysplastic foci are composed of hepatocytes with atypia [1]. The constituent cells are often small, with pleomorphic nuclei, high nuclear/cytoplasmic ratio, and cytoplasmic basophilia, a set of features known as "small cell dysplasia" or "small cell change" [11] (Fig. 1a). The morphologic features of dysplastic foci suggest that they are precursors of early HCC [12]. This view is further supported by studies utilizing comparative genomic hybridization, which have identified similar chromosomal gains and losses in dysplastic foci and nearby HCCs [13, 14].

The precancerous nature of the dysplastic nodules has been documented by a number of studies (reviewed in references [12, 15]). These lesions are classified into two categories: low-grade and high-grade, representing parts of a spectrum that is arbitrarily divided for the purposes of clinical utility [1]. Both low-grade and high-grade dysplastic nodules may contain cells with features suggestive

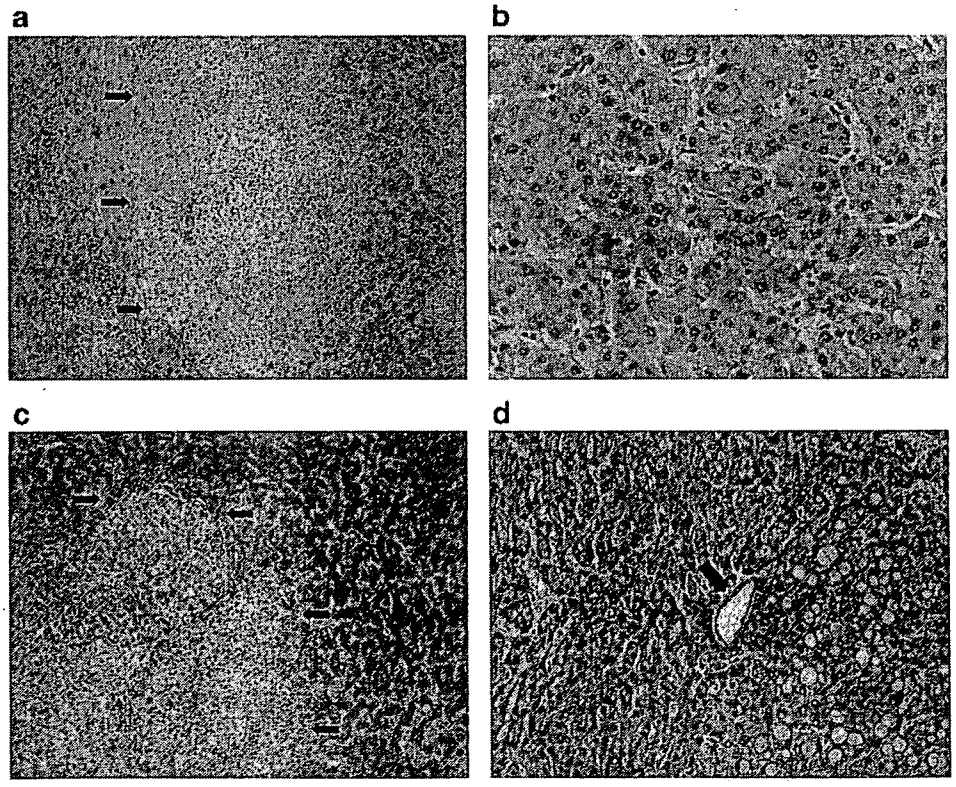

Fig. 1 Examples of dysplastic lesions from cirrhotic livers. **a** Dysplastic focus (*arrows*) in a cirrhotic nodule, composed of small cells arranged in two-cell thick plates. **b** An area from a high-grade dysplastic nodule with thick cell plates and mild nuclear atypia. **c** A high-grade dysplastic nodule containing a subnodule (*arrows*), which is composed of cells with clear cytoplasm (clear cell change). **d** In this high-grade dysplastic nodule, fatty change is seen on the *right*, cell plate thickening is evident on the *left*, and a non-triadal artery is seen in the *center* (*arrow*). Hematoxylin-eosin; **a**, **c**, **d**: 100×; **b**: 400×)

of a clonal population, such as accumulation of fat, hemosiderin or copper [16, 17]. Because low-grade dysplastic nodules lack appreciable cytologic and architectural atypia, their histologic distinction from large regenerative nodules may often be difficult or impossible and will be based on the presence of clone-like populations or unpaired (nontriadal) arteries (see below).

On the other hand, high-grade dysplastic nodules have cytologic and structural features that may be reminiscent of HCC but are insufficient for such diagnosis [1, 18–22]. Mild nuclear atypia, cytoplasmic basophilia or clear change, and increased nuclear/cytoplasmic ratio (as compared to the nearby cirrhotic parenchyma) may be present (Fig. 1b,c). The cell density of these lesions is often in the range of 1.3 to 2 times greater than that of the surrounding parenchyma. The cell plates may be mildly thickened; occasional small pseudoglandular structures may be present; and foci of increased cell proliferation may be evident, forming subnodules within dysplastic nodules (Fig. 1c). Such subnodules may demonstrate fatty change, Mallory-body clustering, or iron resistance when developing within siderotic nodules [19, 23, 24]. Occasional subnodules may display features that are diagnostic of HCC [25, 26].

Dysplastic nodules usually contain portal tracts. In addition, they often contain small numbers of nontriadal (also called "unpaired") arteries (Fig. 1d), a feature that is considered to be indicative of hepatocellular neoplasia (such arteries are characteristically seen in hepatocellular adenomas and carcinomas, but not in cirrhotic nodules) [27–31]. Dysplastic nodules also demonstrate variable degrees of sinusoidal capillarization, which is detectable by immunohistochemical stains for CD31 and CD34 antigens [32–34].

Small hepatocellular carcinomas

By definition, small HCCs measure less than 2 cm in diameter [1]. Careful morphologic studies from Japan have shown that these lesions can be classified into two types: (1) small HCC of indistinctly (vaguely) nodular type and (2) small HCC of distinctly nodular type [1, 20, 35, 36]. On gross pathologic examination, the former type, also known as "early" HCC, is distinguished with difficulty from the surrounding hepatic parenchyma, whereas the latter type is not much different from larger examples of "classic" HCC, despite its small size [3]. Histologic, clinicopathologic and molecular studies suggest that HCCs originate from dysplastic lesions through gradual accumulation of genetic and epigenetic changes [12] (Fig. 2).

On microscopic examination, early HCCs are well-differentiated neoplasms, usually consisting of a relatively uniform population of small cells with nuclear atypia and high nuclear/cytoplasmic ratio, which form irregular, thin trabeculae and pseudoglandular structures (Fig. 3a–c). The cell density within early HCC is at least two times greater than that of the surrounding parenchyma. The tumor cells grow in a replacing fashion, and portal tracts may be present within these lesions. Tumor cell invasion into the intralesional portal tracts (stromal invasion) is frequently seen (Fig. 3c) [36, 37]. This feature is very useful in the differential diagnosis between early HCC and dysplastic

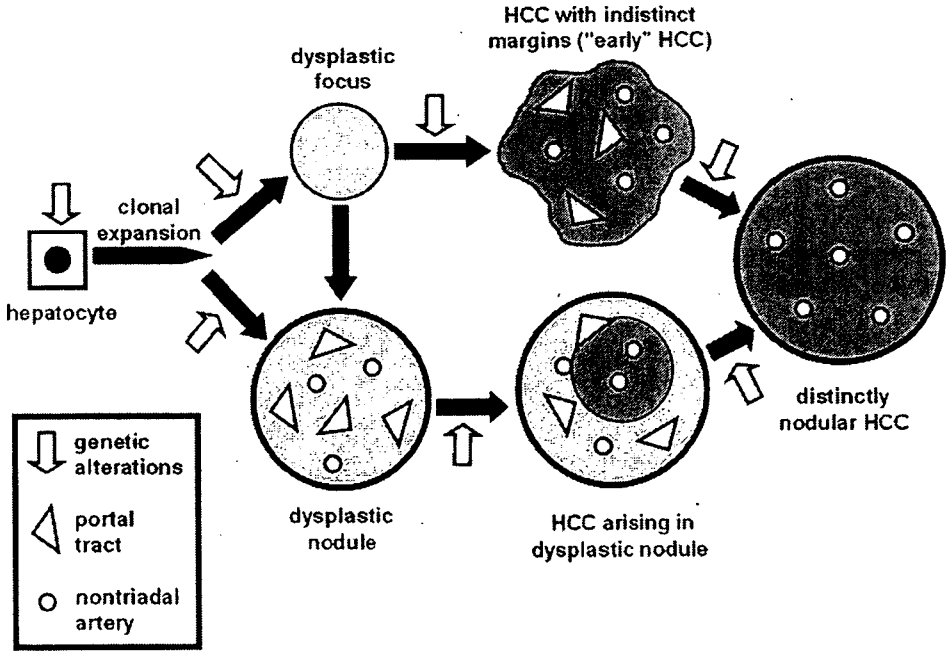

Fig. 2 Precancerous and early cancerous hepatic lesions are the result of accumulating genetic and epigenetic changes, occurring in concert with clonal expansion. A clone originating in a single cell may form a dysplastic focus, while a different clone originating in a different cell may form a dysplastic nodule. Additional molecular changes and clonal expansion result in development of small HCCs. (Reprinted from reference [30] with permission of the publisher, slightly modified)

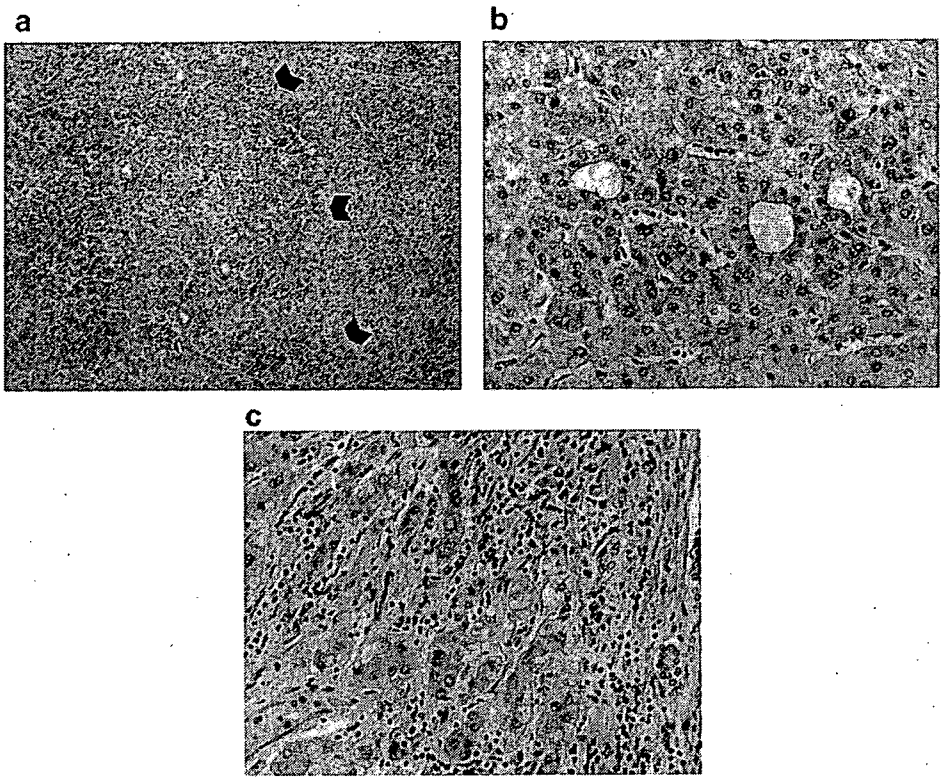

Fig. 3 Typical example of early HCC (this lesion measured 1.3 cm). **a** The margin of the lesion is indistinct (*arrowheads*). The neoplastic cells can be distinguished from the adjacent hepatocytes if attention is paid to cell size, cell crowding, and thickness of cell plates. **b** On high-power examination, the neoplastic cells are seen with increased nuclear/cytoplasmic ratio and mild nuclear atypia to be arranged in irregular thin trabeculae and pseudoglandular stractures. **c** Invasion of portal tracts by neoplastic cells is a diagnostically helpful feature. Hematoxylin-eosin; **a** 100×; **b**, **c**: 400×

nodule. Detection of heat shock protein-70 and glypican-3 by immunohistochemical stains has been suggested as a useful adjunct in distinguishing early HCC from dysplastic nodules [38, 39].

Early HCCs receive blood supply from two sources: vessels of entrapped portal tracts (branches of the hepatic artery and portal vein), as well as newly formed (nontriadal) arteries. However, the number of intratumoral portal tracts is less than one-third of that in the surrounding liver tissue, while the nontriadal arteries of these lesions are insufficiently developed [3, 36]. Therefore, cell crowding and low blood supply may result in hypoxia, providing a possible explanation for the common occurrence of steatosis in these lesions [40]. The degree of sinusoidal capillarization in early HCCs is similar to that of high-grade dysplastic nodules. Sometimes, nodular aggregates of less differentiated tumor cells are seen to arise within the well-differentiated cell population of early HCCs [41].

Small HCCs of distinctly nodular type are well-demarcated, often encapsulated nodules (Fig. 4a). Approxi-

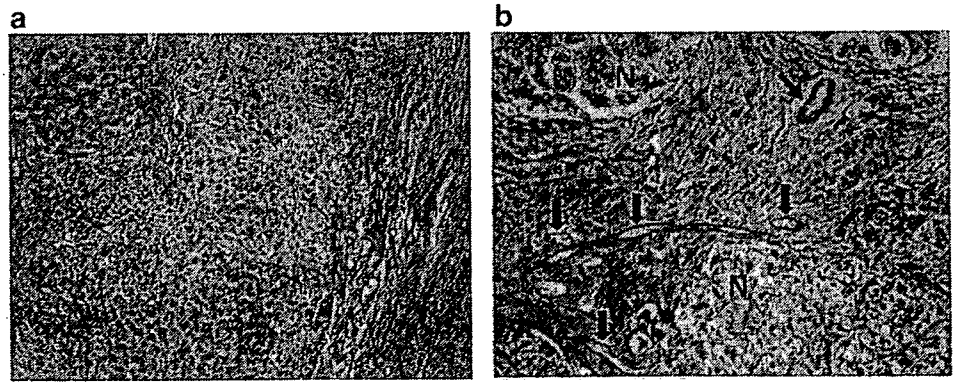

Fig. 4 Typical example of small HCC of distinctly nodular type (this lesion measured 1.8 cm). **a** The tumor is surrounded by a band of fibrous tissue, i.e., a pseudocapsule, seen on the *right*. The lesional cells in this peripheral area are well-differentiated. **b** In other parts of the lesion, subnodules (*N*) of moderately differentiated tumor cells with basophilic or clear cytoplasm are evident. Nontriadal arteries are easily identified (*arrows*). Hematoxylin-eosin, 100×

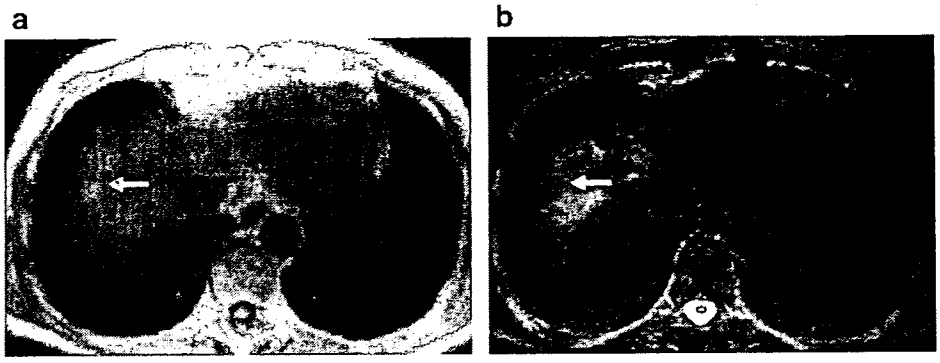

Fig. 5 A high-grade dysplastic nodule in segment 8 (*arrow*) demonstrates high signal on a T1-weighted image (**a**) and low signal on a T2-weighted image (**b**)

mately 80% of these lesions are moderately differentiated histologically, the remaining containing both moderately and well-differentiated areas [3, 35, 36]. Therefore, small HCCs of distinctly nodular type are similar to larger examples of classic HCC not only at the macroscopic, but also at the microscopic, level. In these lesions, more than one histologically distinct cell population may be encountered, and nodule-in-nodule growth patterns are frequent (Fig. 4b). The pattern of cell growth may be trabecular, compact, or scirrhous. Portal tracts are not present within small HCCs of distinctly nodular type, whereas nontriadal arteries are often plentiful (Fig. 4b), and sinusoidal capillarization is well-developed. Therefore, the blood supply of these lesions is basically derived from nontriadal arteries [36]. Tumor cell invasion into portal vein branches and minute intrahepatic metastases are observed in 27 and 10% of cases, respectively [35].

Imaging findings of precancerous nodules and small hepatocellular carcinomas and their histologic correlation

Presently, there is ongoing research for better hepatocellular nodule detection and characterization because identification of HCC at an early stage is critical for prompt surgical resection, transplantation, or local ablation therapy to ensure a better chance for treatment [42, 43]. However, imaging findings are not always conclusive, among other reasons because cirrhosis limits the sensitivity and specificity of any imaging modality in the detection and characterization of focal liver lesions more than any other diffuse liver disease. Liver inhomogeneity due to fibrosis leads to heterogeneous CT attenuation and MR signal intensity, significantly impairing lesional visibility [44–46]. In addition, the change in distribution of blood flow in the cirrhotic liver creates patterns of heterogeneous parenchymal enhancement that can be confused with a neoplastic lesion [47–50]. On the other hand, percutaneous needle biopsy to obtain a reliable tissue sample from a particular nodule "hidden" within a cirrhotic liver may be technically challenging [51, 52]. Therefore, the search for imaging findings considered most typical for small HCC (i.e., HCC measuring less than 2 cm in diameter) is of outmost importance.

Unfortunately, previously described MRI findings considered relatively specific for HCC, such as internal mosaic architecture—reflected by enhancement inhomogeneities—as well as capsule formation, are infrequently seen on imaging of small HCCs [53]. Similarly, small HCCs demonstrate a variety of T1- and T2-weighted signal intensities, making a specific diagnosis of HCC arising in cirrhosis very difficult [54]. However, hyperintensity on T1-weighted MR images practically narrows

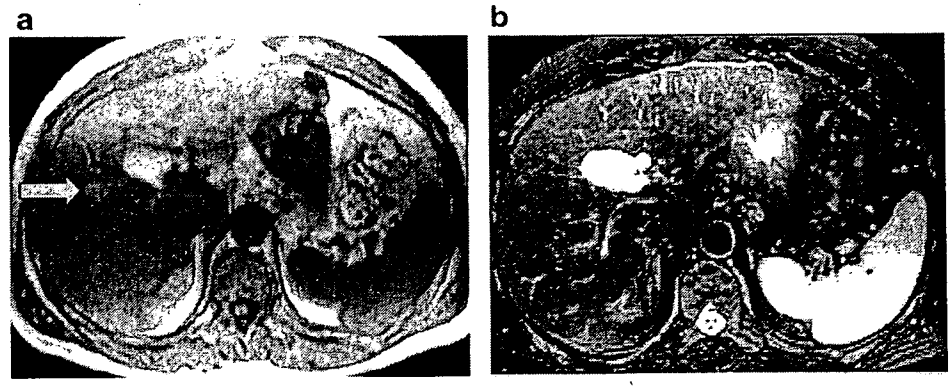

Fig. 6 Early HCC presenting as hyperintense nodule (*arrow*) on T1-weighted image (**a**) and as isointense nodule on T2-weighted image (**b**)

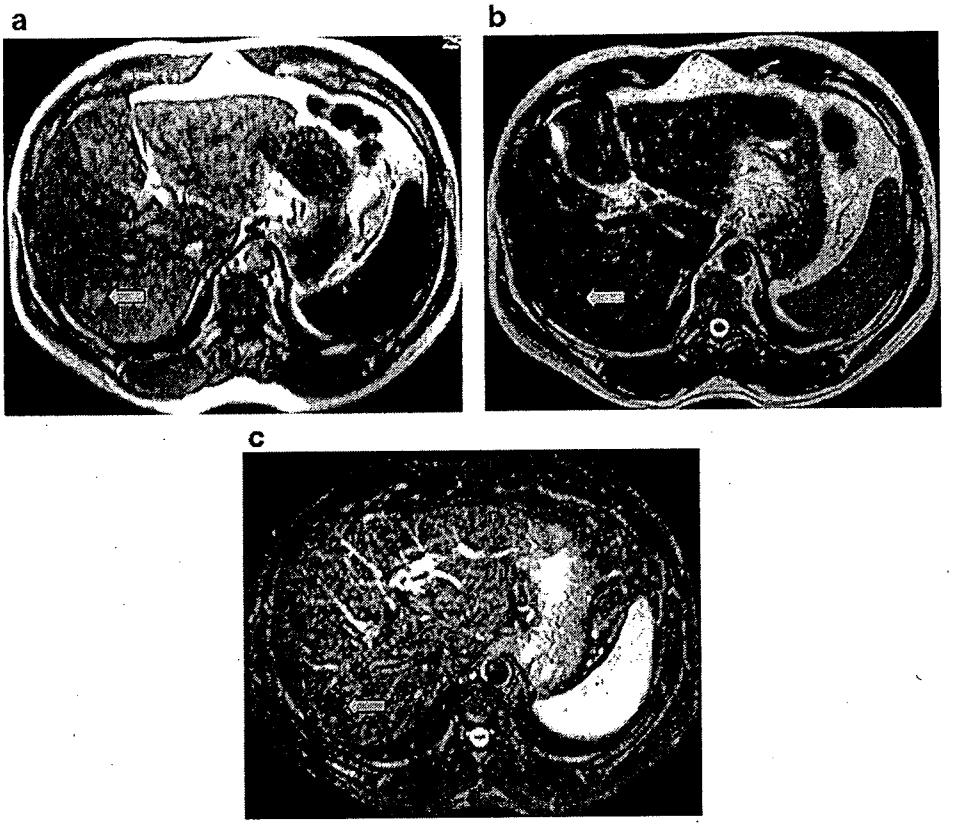

Fig. 7 MR findings for a fat-containing, early HCC in a patient with cirrhosis due to chronic hepatitis B. The nodule (*arrow*) appears hyperintense on T1-weighted image (**a**), remains slightly hyperintense on T2-weighted image (**b**) and becomes hypointense on fat-saturated (SPIR sequence) image (**c**)

the differential diagnosis of a newly detected nodule to only two possibilities: a high-grade dysplastic nodule or an early HCC [53, 55]. In this setting, T2-weighted images may aid in further differentiating these two lesions, since dysplastic nodules are usually of low signal intensity on T2-weighted images (Fig. 5a,b), while early HCCs are typically either isointense (Fig. 6a,b) or slightly hyperintense (Fig. 7a,b).

In the series published by Kadoya et al. [53], all six well-differentiated HCCs, defined as grade 1 by the Edmondson system [56], were hyperintense on T1-weighted MR images, regardless of the presence of fat within the tumor cells. Conversely, hyperintensity on T2-weighted MR images—associated with a variety of signal intensities on T1-weighted images—was observed in all grade 2–4 tumors in the same series [53]. According to our experience as well as that of others, the frequency of hyperintensity on T1-weighted images is much higher in well-differentiated (grade 1) tumors [20, 53, 57] (Figs. 6, 7). In contrast, hyperintensity on T2-weighted images is substantially more frequent—although not specific—in classic (above grade 1) HCCs (Fig. 8).

Fat-containing HCCs (a histologic finding mostly associated with well-differentiated tumors) also appear

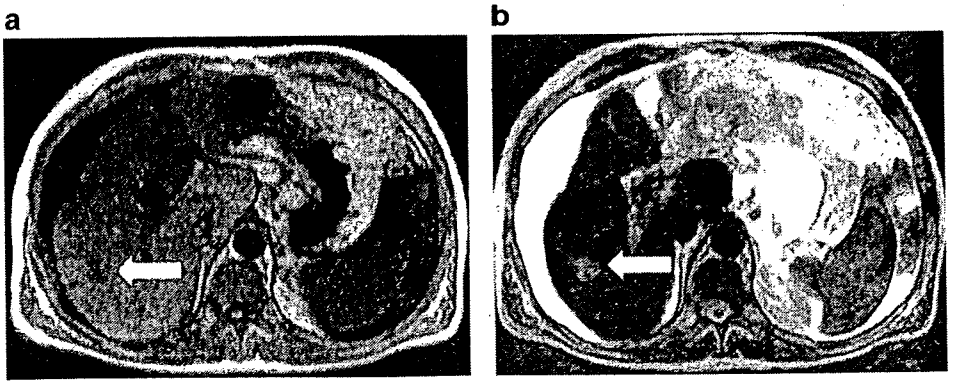

Fig. 8 Small, moderately differentiated HCC (*arrow*) demonstrating a typical combination of low signal on T1-weighted image (**a**), and high signal on T2-weighted image (**b**)

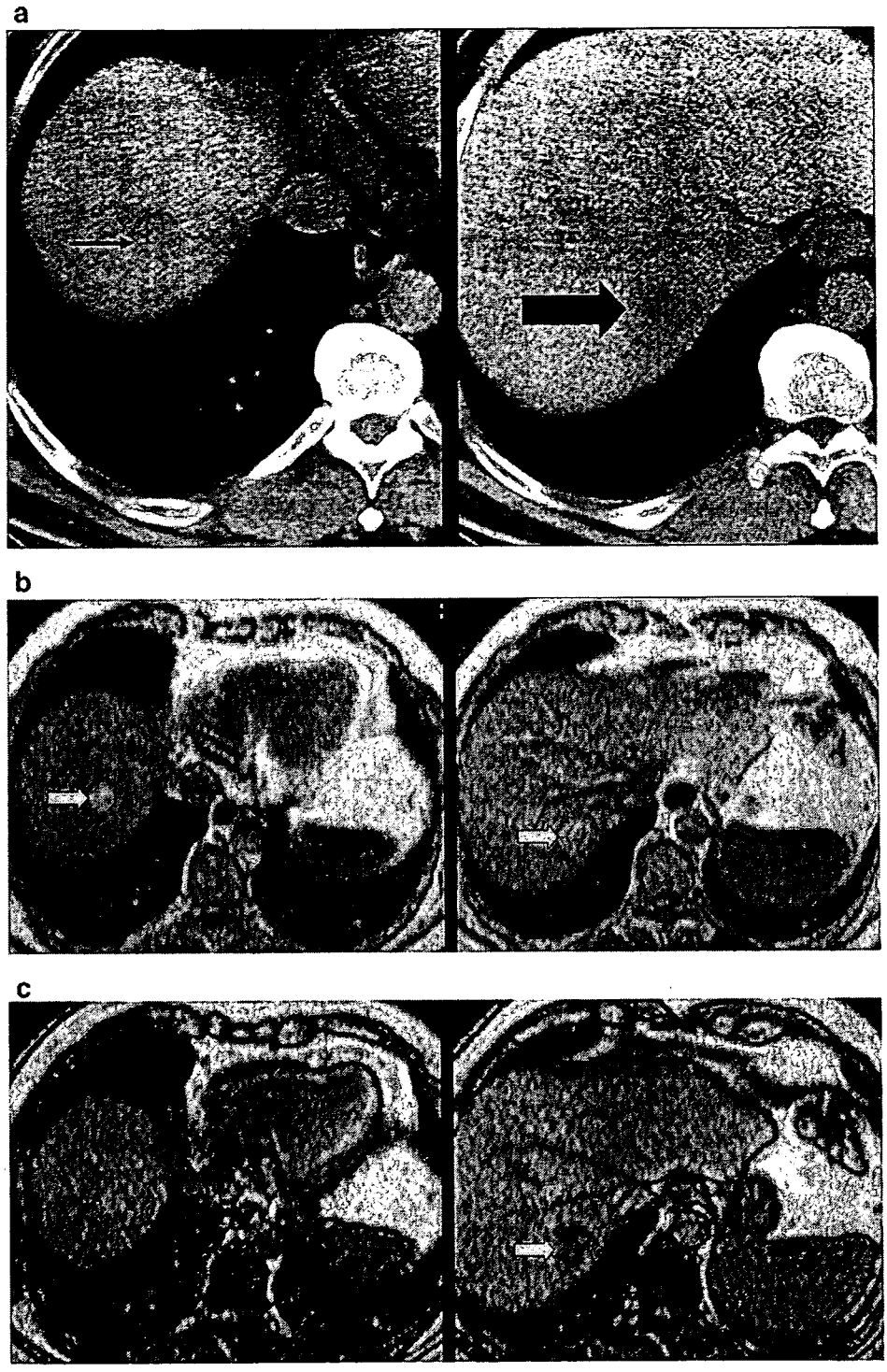

Fig. 9 Two fat-containing early HCCs in a patient with cirrhosis due to chronic viral hepatitis B. a Unenhanced CT demonstrates two low-density lesions in segments 8 (*small arrow*) and 7 (*large arrow*). The lesions became isodense in the arterial phase and remained so in the portal venous phase (not shown). On in-phase T1-weighted gradient-echo sequence (b), the lesions are hyperintense (*arrows*), while on out-of-phase images (c), they lose signal, becoming iso- and hypointense (*arrow*), respectively

hyperintense on T1-weighted images (Figs. 7, 9). Chemical shift imaging using phase-contrast, gradient-echo technique can help make a specific diagnosis of fat-containing HCC (Fig. 9). Finally, increased signal intensity of a nodule on both T1- and T2-weighted images makes HCC the most likely diagnosis [48].

A significant number of older and more recent publications have attempted to correlate the histologic features of

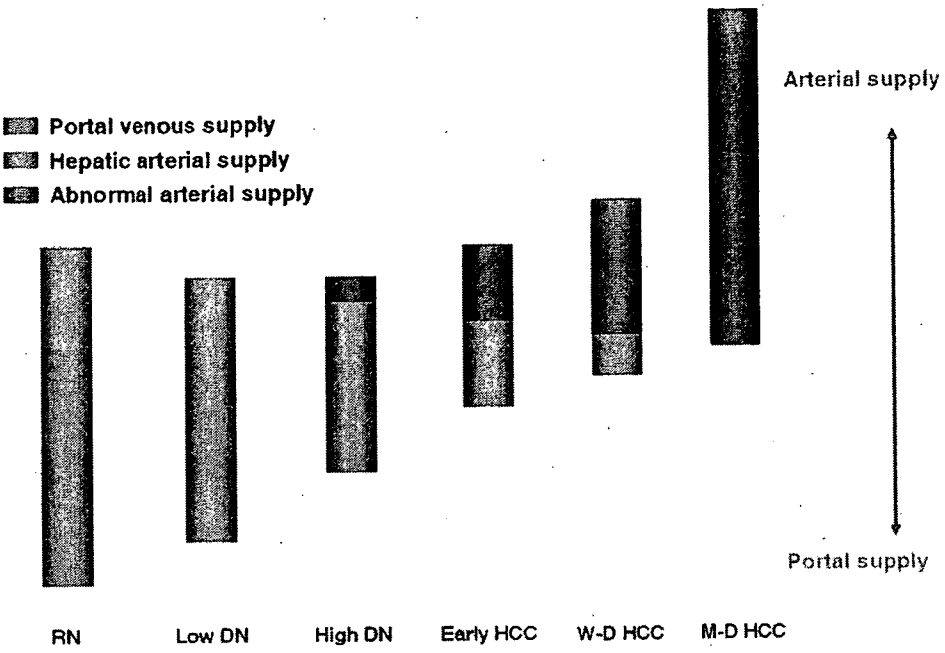

Fig. 10 Diagram showing differences in blood supply among the various nodular lesions arising in the process of hepatocarcinogenesis. *RN* Large regenerative nodule, *DN* dysplastic nodule, *W-D* well differentiated, *M-D* moderately differentiated

the spectrum of nodules arising in the process of hepatocarcinogenesis with their CT and MR findings, before and after i.v. contrast administration. Features such as cell crowding, tumor necrosis, structural pattern (trabecular, pseudoglandular or scirrhous), accumulation of fat, hemosiderin or copper, presence of portal tracts or nontriadal arteries, and degree of sinusoidal capillarization, all have been implicated to explain the variety of MR signal intensities, CT attenuation coefficients, and enhancement patterns encountered in the evaluation of nodules arising in cirrhosis [53, 55, 57–60]. Matsui et al. [55], correlating MR signal intensity characteristics of high-grade dysplastic nodules and early HCCs with their histologic background, considered cell crowding (accompanied by decreased sinusoidal space), fat accumulation (occurring in one-third of the cases) and, possibly, copper deposition, to be responsible for hyperintensity on T1-weighted images (Figs. 7, 9), while decreased blood supply and/or reduced sinusoidal space was thought to be the cause of hypo- or isointensity on T2-weighted images.

Regarding the blood supply, three types of feeding vessels can be recognized in large nodules, as described above: (1) branches of the hepatic artery, (2) branches of the portal vein, and (3) abnormal (nontriadal) arteries [27–31]. The proportion of blood supply derived from each type of vessel differs in accordance with the presence and grade of malignancy in each particular nodule. This has been shown by the work of Hayashi et al. [6], indicating that when HCC emerges in a cirrhotic liver, the intranodular normal portal and arterial supply gradually decreases, whereas the abnormal arterial supply provided by nontriadal arteries increases, following the increase in the grade of malignancy of the nodule (Fig. 10). These fine changes in intranodular supply can be better demonstrated at CTAP and CTHA (Fig. 11).

The same investigators in a more recent report [61] evaluated the progression of 176 nodular lesions with features of dysplastic nodule or early HCC from 49 consecutive cirrhotic patients by repeat CTAP and/or CTHA. On the basis of CTHA findings, the lesions were

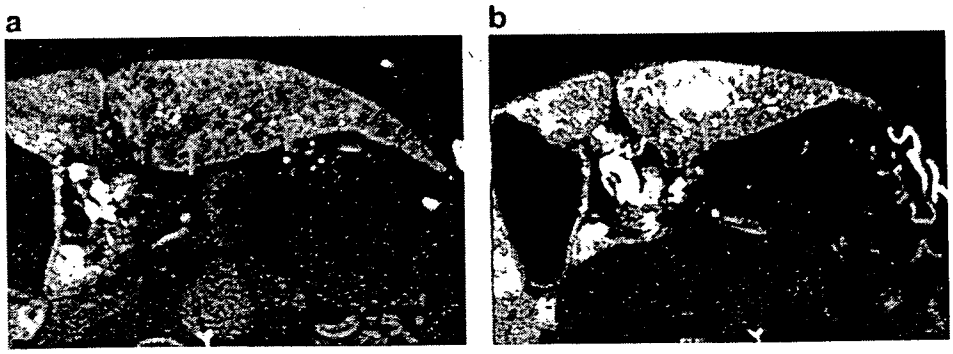

Fig. 11 CTHA showing progression of a nodule (**a**) to a hypervascular HCC (**b**) observed within a period of less than 3 years. The lesion originally demonstrated decreased arterial supply (*arrow* in **a**) and became hypervascular when it transformed to a classic HCC (*arrow* in **b**)

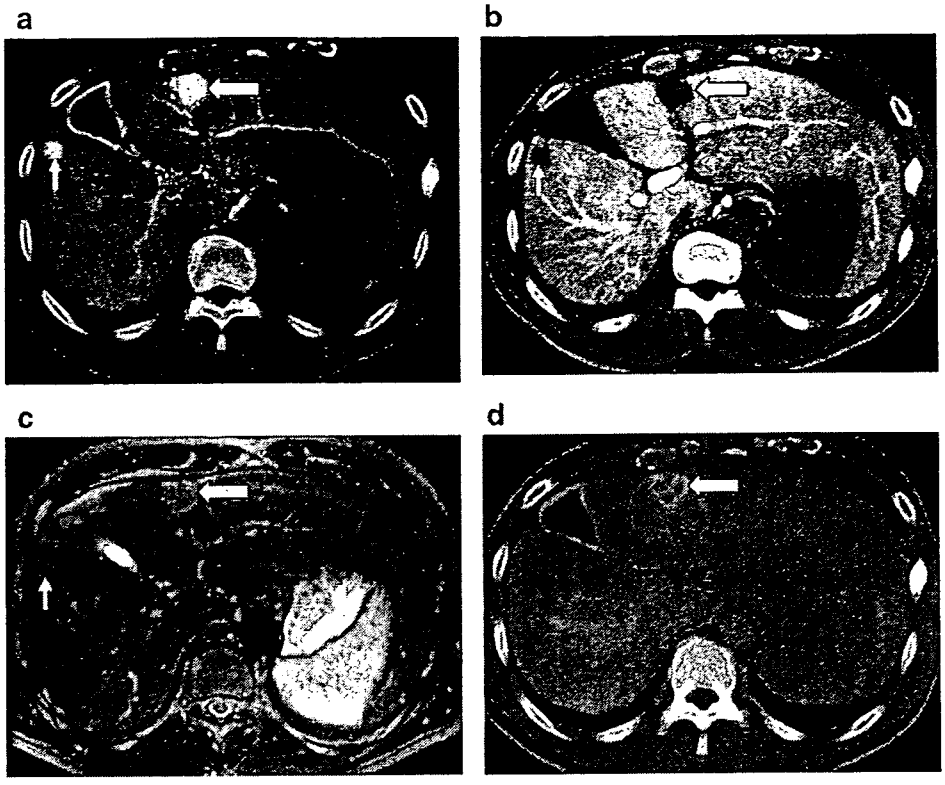

Fig. 12 a Two nodules (*arrows*) demonstrate homogeneous enhancement on CTHA (group IV), indicating generalized increased arterial supply. On CTAP (**b**), the nodules are strongly hypoattenuating (group D), indicating absence of portal supply. Both lesions are hyperintense on a T2-weighted image (**c**), which is expected in about 85% of nodules demonstrating this combination of contrast enhancement. The bigger nodule (*arrow* in **d**) demonstrates the "corona pattern" of perilesional enhancement during the washout phase of this lesion

categorized into four groups (groups I-IV) with group I nodules being isoattenuating (not visualized), indicating the presence of almost the same arterial blood supply in the nodule and in the surrounding liver parenchyma, and group IV nodules being hyperattenuating, indicating a generalized increased intranodular arterial blood supply (Fig. 12a). Groups II and III nodules had intermediate attenuation levels.

Likewise, the nodules were classified into four groups based on CTAP findings (groups A–D), whereby group A nodules were isoattenuating (not visualized), indicating an almost identical intranodular portal blood supply as the surrounding liver, and group D nodules were markedly

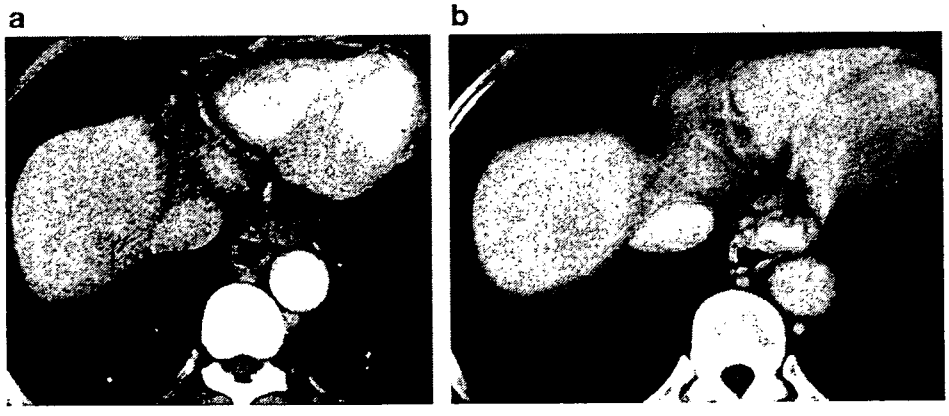

Fig. 13 Multiphase CT obtained 2 months prior to transplantation of a patient with chronic hepatitis B demonstrates the nodule-in-nodule enhancement pattern that is characteristic of classic HCC developing within an early HCC or a dysplastic nodule. **a** Faint enhancement (*arrow*) of the developing nodular HCC on arterial phase. **b** On the portal venous phase, the arterial enhancement disappears and the whole lesion becomes hypoattenuated. (From reference [65] with permission from the publisher)

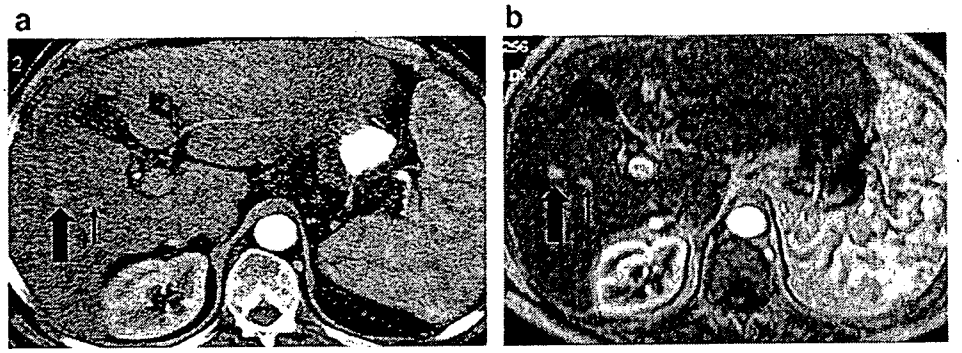

Fig. 14 Patients with cirrhosis due to chronic hepatitis C. There are two small hypervascular lesions (*arrows*), which were demonstrated only in the early arterial phase of a multiphase MDCT study (**a**) and on a post-i.v. Gd injection dynamic MR examination (**b**). The second lesion (*small arrow*) is better delineated on the dynamic MR examination. In the explanted liver, both lesions measured less than 1.8 cm, and their histologic examination revealed moderately differentiated HCC of the distinctly nodular type

hypoattenuating indicating an absent intranodular portal venous supply (Fig. 12b), while group B and C nodules had intermediate features.

In this study [61], significant correlations were observed between the four groups of nodules as classified on CTAP and CTHA findings, and the presence and grade of malignancy as determined by clinical and radiologic follow-up. More specifically, there were statistically significant correlations between moderately and poorly differentiated HCCs with group D or group IV nodules, while dysplastic nodules and well-differentiated HCCs tended to appear in groups I–III or A–C respectively, with varying degrees of overlap.

These findings correspond well with the histologic observations of Nakashima et al. [36], describing few portal tracts in early HCCs (numbering approximately one-third of those in the surrounding liver parenchyma) and insufficiently developed nontriadal arteries, as opposed to absence of portal tracts and presence of well-developed nontriadal arteries in small HCCs of the distinctly nodular type. These fine intranodular changes in arterial supply, although better demonstrated by CTAP and CTHA, can also be demonstrated by noninvasive methods, such as dynamic CT, dynamic MRI, Doppler or contrast-enhanced US (Figs. 13, 14) [5, 9, 62, 63]. However, the slight changes in portal supply cannot be accurately evaluated by noninvasive techniques—a possible exemption might be contrast-enhanced US [63, 64]—therefore, CTAP may be necessary for evaluation.

Furthermore, recent reviews on blood supply of nodular lesions in cirrhosis indicate a correlation between attenuation characteristics at CTHA and CTAP on one hand, and MR signal intensity on T2-weighted images on the other [57]. More specifically, nodules hypoattenuating at CTHA and isoattenuating at CTAP were hypointense on T2-weighted MR images in more than 70% of cases, while nodules hyperattenuating at CTHA and strongly hypoattenuating at CTAP were hyperintense on T2-weighted MR images in 85% of cases (Fig. 12). These observations make it reasonable to assume that the enhancement pattern of a nodule and its signal-intensity characteristics on T2-weighted MR images are interrelated and may reflect histologic changes in the process of the malignant transformation of a dysplastic nodule to HCC.

It has been speculated that the hypercellularity present in dysplastic nodules narrows the sinusoidal spaces resulting in decreased nodular blood volume relative to the surrounding liver parenchyma and leading to hypointensity on T2-weighted MR images [19]. In contrast, the progressive increase in the number of nontriadal arteries, as the HCC size and grade of malignancy increase [54, 60], leads to an increase in the

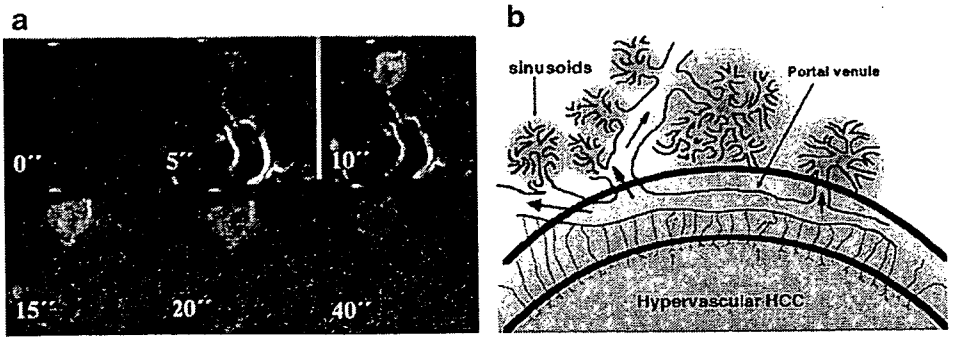

Fig. 15 **a** Single-level dynamic CTHA demonstrates the "corona pattern" of drainage of a hypervascular HCC at 0, 5, 10, 15, 20 and 40 s after the start of the intrarterial injection. **b** Schematic presentation of blood drainage from a hypervascular HCC

Table 1 Imaging features of small HCC

A. Early HCC (small HCC with indistinct margins)
Small indistinct nodule
Relative arterial hypovascularity
Decreased intranodular portal supply
Hyperintensity on T1-weighted, isointensity or hypointensity on T2-weighted MR images
Occasional fatty changes
Occasional "nodule-in-nodule" appearance (when "classic" HCC emerges within early HCC)
Accumulation of SPIO or ultrasound contrast media
B. "Classic" small HCC (small HCC with distinct margins)
Capsule formation and mosaic architecture
Relative arterial hypervascularity
Corona pattern of enhancement
Occasional fatty changes
Occasional "nodule-in-nodule" appearance
Hyperintensity on T1- and T2-weighted MR images
Tumor thrombus in portal or hepatic veins

size of the blood spaces, resulting in hyperintensity on T2-weighted MR images. However, the exact histologic background responsible for the MR signal-intensity characteristics of different types of HCCs remains elusive.

Of particular interest are two enhancement patterns that are quite specific for a small HCC: the "nodule-in-nodule" configuration and the "corona enhancement." The nodule-in-nodule configuration corresponds to the nodule-in-nodule growth pattern seen on histologic examination and implies the emergence of a nodular-type HCC developing within and replacing part of a dysplastic nodule or an early HCC [65]. This sign refers to a liver nodule usually bigger than 1.0 cm, a portion of which is not enhancing during the hepatic arterial phase of a dynamic CT, MRI, or CTHA study, corresponding to either a dysplastic nodule or early HCC tissue. The nodule contains a smaller nodule that enhances on the arterial phase (increased arterial supply) and corresponds to a developing, distinctly nodular-type HCC (Fig. 13). Another expression of this sign is the "hypervascular focus sign" described by Hayashi and his associates [6]. This complex pattern of enhancement within the same nodule conforms well with the stepwise process of hepatocarcinogenesis but is not frequently demonstrated. In our experience, its reported frequency does not exceed 6% of the cases on dynamic CT or MR [65].

The corona pattern of perinodular enhancement [66] refers to the liver parenchymal enhancement adjacent to the HCC during the wash-out phase of the lesion at a single-level dynamic CTHA and apparently reflects the mode of drainage of a small hypervascular HCC of the distinctly nodular type (Figs. 12d, 15a,b). This relatively specific finding can also be seen in other hypervascular lesions, such as hypervascular metastases, hepatic adenomas and hyperplastic nodules in alcoholic cirrhosis.

In the process of making the diagnosis of nodular lesions in cirrhosis, it should be kept in mind that hepatocarcinogenesis is a continuous process and has been arbitrarily divided by the researchers into steps for the purposes of better understanding and investigation. Therefore, the evolving histologic features of nodular lesions during this process, including changes in blood supply, fat deposition, copper accumulation, siderosis, or iron resistance, are responsible for significant overlap in enhancement patterns and MR signal intensities on T1- and T2-weighted images, sometimes making the differential diagnosis of hepatocellular nodules extremely difficult, both by imaging and histologic criteria. Moreover, reported discrepancies in enhancement patterns and signal intensities of dysplastic nodules and small HCCs may also in part be attributed to different histologic criteria used to characterize large nodules by pathologists in different countries, as well as to changes in nomenclature over time. As international consensus regarding classification and nomenclature of these lesions is developing [3, 67, 68], it is hoped that such discrepancies will be minimized in the future.

From a practical point of view, there are two areas in the spectrum of hepatocellular nodules where most of the discrepancies of pathologic-imaging correlation are reported to occur in clinical practice: (1) differential diagnosis between a high-grade dysplastic nodule and an early HCC, and (2) differential diagnosis between an early HCC and a small HCC of the distinctly nodular type [69]. In the first case, the difficulties arise from the radiologic and histologic similarities of the two lesions, which are defined differently, whereas in the second case, two histologically distinct lesions are both designated as small HCC in the current classification [1]. Imaging differentiation between such lesions may be very difficult, and this may be compounded by developing, and therefore not widely accepted, concepts, terms, and definitions.

More specifically, because of the histologic similarities between high-grade dysplastic nodules and early HCCs, these lesions may display overlapping findings on T1- and T2-weighted MR images (compare images of Fig. 5a,b with images of Fig. 6a,b) and in post-i.v. contrast enhancement. Such histologic features that vary from case to case include (1) increased cell density, (2) fat accumulation, (3) presence of portal tracts, (4) presence of a small number of nontriadal arteries, and (5) partially developed sinusoidal capillarization. Therefore, it is not surprising that pathologists outside of Japan only recently have realized the existence of early HCC as a lesion distinct from the dysplastic nodule [68].

On the other hand, histologic features characterizing HCC of the distinctly nodular type, such as (1) well-developed nontriadal arteries, (3) well-developed capillar-

ization, (3) pseudocapsule, and (4) complete absence of portal tracts, are not seen in early HCC and therefore may produce diverse imaging findings in two histologically and biologically different lesions, both designated currently as small HCC. In fact, evidence accumulated thus far suggests that, similar to dysplastic nodules, early HCC does not have the capability to produce metastases, as opposed to small HCC of distinctly nodular type [3]. However, because HCC of distinctly nodular type may arise within early HCC, on tabulating the imaging features of these two types of small HCC, we must allow for a certain degree of overlap (Table 1).

In conclusion, characterization of nodules arising in cirrhosis by imaging methods can be a very difficult task in clinical practice. The nodular lesions that emerge in the process of hepatocarcinogenesis, i.e., the dysplastic nodules, the early HCCs, and the classic small HCCs, may demonstrate overlapping findings. Relatively specific radiologic findings are few and not frequently encountered, especially in nodules measuring less than 1.5 cm in diameter. The importance of pathologic-imaging correlation cannot be overemphasized, not only on a daily diagnostic basis, but also for the overall understanding and advancement of this field.

References

1. International Working Party (1995) Terminology of nodular hepatocellular lesions. Hepatology 22:983–993
2. Thorgeirsson SS, Grisham JW (2002) Molecular pathogenesis of human hepatocellular carcinoma. Nat Genet 31:339–346
3. Kojiro M, Roskams T (2005) Early hepatocellular carcinoma and dysplastic nodules. Semin Liver Dis 25:133–142
4. Matsui O, Kadoya M, Kameyama T et al (1991) Benign and malignant nodules in cirrhotic livers: distinction based on blood supply. Radiology 178:493–497
5. Schima W, Hammerstingl R, Catalano C et al (2006) Quadruple - phase MDCT of the liver in patients with suspected hepatocellular carcinoma: effect of contrast material flow rate. AJR Am J Roentgenol 186:1571–1579
6. Hayashi M, Matsui O, Ueda K et al (1999) Correlation between the blood supply and grade of malignancy of hepatocellular nodules associated with liver cirrhosis: evaluation by CT during intra arterial injection of contrast medium. AJR Am J Roentgenol 172:969–976
7. Kwak HS, Lee JM, Kim CS (2004) Preoperative detection of hepatocellular carcinoma: comparison of combined contrast-enhanced MR imaging and combined CT during arterial portography and CT hepatic arteriography. Eur Radiology 14:447–457
8. Kim YK, Kwak HS, Kim CS (2005) Hepatocellular carcinoma in patients with chronic liver disease: comparison of SPIO-enhanced MR imaging and 16-detector row CT. Radiology 238:531–541
9. Simon G, Link TM, Wortler K et al (2005) Detection of hepatocellular carcinoma: comparison of Gd-DTPA- and ferumoxides-enhanced MR imaging. Eur Radiol 15:895–903
10. Wilson SR, Burns PN (2006) An algorithm for the diagnosis of focal liver masses using microbubble contrast-enhanced pulse-inversion sonography. AJR Am J Roentgenol 186:1401–1412
11. Watanabe S, Okita K, Harada T et al (1983) Morphologic studies of the liver cell dysplasia. Cancer 51:2197–2205
12. Hytiroglou P (2004) Morphological changes of early human hepatocarcinogenesis. Semin Liver Dis 24:65–75
13. Zondervan PE, Wink J, Alers JC et al (2000) Molecular cytogenetic evaluation of virus-associated and non-viral hepatocellular carcinoma: analysis of 26 carcinomas and 12 concurrent dysplasias. J Pathol 192:207–225
14. Marchio A, Terris B, Meddeb M et al (2001) Chromosomal abnormalities in liver cell dysplasia detected by comparative genomic hybridization. Mod Pathol 54:270–274
15. Libbrecht L, Desmet V, Roskams T (2005) Preneoplastic lesions in human hepatocarcinogenesis. Liver Int 25:16–27
16. Terada T, Nakanuma Y, Hoso M et al (1989) Fatty macroregenerative nodule in non-steatotic liver cirrhosis. A morphologic study. Virchows Arch A Pathol Anat Histopathol 415:131–136
17. Terada T, Nakanuma Y (1989) Survey of iron-accumulative macroregenerative nodules in cirrhotic livers. Hepatology 10:851–854
18. Furuya K, Nakamura M, Yamamoto Y et al (1988) Macroregenerative nodule of the liver. A clinicopathologic study of 345 autopsy cases of chronic liver disease. Cancer 61:99–105
19. Nakanuma Y, Terada T, Terasaki S et al (1990) 'Atypical adenomatous hyperplasia' in liver cirrhosis: low-grade hepatocellular carcinoma or borderline lesion? Histopathology 17:27–35
20. Sakamoto M, Hirohashi S, Shimosato Y (1991) Early stages of multistep hepatocarcinogenesis: adenomatous hyperplasia and early hepatocellular carcinoma. Hum Pathol 22:172–178
21. Terada T, Terasaki S, Nakanuma Y (1993) A clinicopathologic study of adenomatous hyperplasia of the liver in 209 consecutive cirrhotic livers examined by autopsy. Cancer 72:1551–1556
22. Hytiroglou P, Theise ND, Schwartz M et al (1995) Macroregenerative nodules in a series of adult cirrhotic liver explants: issues of classification and nomenclature. Hepatology 21:703–708
23. Terada T, Hoso M, Nakanuma Y (1989) Mallory body clustering in adenomatous hyperplasia in human cirrhotic livers: report of four cases. Hum Pathol 20:886–890
24. Terada T, Nakanuma Y (1989) Iron-negative foci in siderotic macroregenerative nodules in human cirrhotic liver. A marker of incipient neoplastic lesions. Arch Pathol Lab Med 113:916–920
25. Arakawa M, Kage M, Sugihara S et al (1986) Emergence of malignant lesions within an adenomatous hyperplastic nodule in a cirrhotic liver. Observations in five cases. Gastroenterology 91:198–208
26. Ohno Y, Shiga J, Machinami R (1990) A histopathological analysis of five cases of adenomatous hyperplasia containing minute hepatocellular carcinoma. Acta Pathol Jpn 40:267–278

27. Wada K, Kondo F, Kondo Y (1988) Large regenerative nodules and dysplastic nodules in cirrhotic livers: a histopathologic study. Hepatology 8:1684–1688
28. Ueda K, Terada T, Nakanuma Y, Matsui O (1992) Vascular supply in adenomatous hyperplasia of the liver and hepatocellular carcinoma. A morphometric study. Hum Pathol 23:619–626
29. Terada T, Nakanuma Y (1995) Arterial elements and perisinusoidal cells in borderline hepatocellular nodules and small hepatocellular carcinomas. Histopathology 27:333–339
30. Park YN, Yang CP, Fernandez GJ et al (1998) Neoangiogenesis and sinusoidal "capillarization" in dysplastic nodules of the liver. Am J Surg Pathol 22:656–662
31. Roncalli M, Roz E, Coggi G et al (1999) The vascular profile of regenerative and dysplastic nodules of the cirrhotic liver: implications for diagnosis and classification. Hepatology 30:1174–1178
32. Bhattacharya S, Davidson B, Dhillon AP (1995) Blood supply of early hepatocellular carcinoma. Semin Liver Dis 15:390–401
33. Park YN, Kim YB, Yang KM, Park C (2000) Increased expression of vascular endothelial growth factor and angiogenesis in the early stage of multistep hepatocarcinogenesis. Arch Pathol Lab Med 124:1061–1065
34. Frachon S, Gouysse G, Dumortier J et al (2001) Endothelial cell marker expression in dysplastic lesions of the liver: an immunohistochemical study. J Hepatol 34:850–857
35. Nakashima O, Sugihara S, Kage M, Kojiro M (1995) Pathomorphologic characteristics of small hepatocellular carcinoma: a special reference to small hepatocellular carcinoma with indistinct margins. Hepatology 22:101–105
36. Nakashima Y, Nakashima O, Hsia CC et al (1999) Vascularization of small hepatocellular carcinomas: correlation with differentiation. Liver 19:12–18
37. Kondo F, Kondo Y, Nagato Y et al (1994) Interstitial tumour cell invasion in small hepatocellular carcinoma. Evaluation in microscopic and low magnification views. J Gastroenterol Hepatol 9:604–612
38. Chuma M, Sakamoto M, Yamazaki K et al (2003) Expression profiling in multistage hepatocarcinogenesis: identification of HSP70 as a molecular marker of early hepatocellular carcinoma. Hepatology 37:198–207
39. Llovet J, Chen Y, Wurmbach E et al (2006) A molecular signature to discriminate dysplastic nodules from early hepatocellular carcinoma in HCV cirrhosis. Gastroenterology 131:1758–1767
40. Kutami R, Nakashima Y, Nakashima O et al (2000) Pathomorphologic study on the mechanism of fatty change in small hepatocellular carcinoma of humans. J Hepatol 33:282–289
41. Kojiro M, Nakashima O (1999) Histopathologic evaluation of hepatocellular carcinoma with special reference to small early stage tumors. Semin Liver Dis 19:287–296
42. Bigourdan JM, Jaeck D, Meyer N et al (2003) Small hepatocellular carcinoma in Child A cirrhotic patients: hepatic resection versus transplantation. Liver Transpl 9:513–520
43. Llovet JM (2005) Updated treatment approach to hepatocellular carcinoma. Gastroenterol 40:225–235
44. Miller WJ, Baron RL, Dodd GD et al (1994) Malignancies in patients with cirrhosis: CT sensitivity and specificity in 200 consecutive patients. Radiology 193:645–650
45. Lucidarme O, Baleston F, Cadi M et al (2003) Non-invasive detection of liver fibrosis: is superparamagnetic iron oxide particle-enhanced MR imaging a contributive technique? Eur Radiol 13:467–474
46. Aguirre DA, Behling CA, Alpert E et al (2006) Liver fibrosis: noninvasive diagnosis with double contrast material - enhanced MR imaging. Radiology 239:425–437
47. Itai Y, Matsui O (1997) Blood flow and liver imaging. Radiology 202:306–314
48. Baron RL, Peterson MS (2001) Screening the cirrhotic liver for hepatocellular carcinoma with CT and MR imaging: opportunities and pitfalls. Radiographics 21:S117–S132
49. Kanematsu M, Kondo H, Semelka RC et al (2003) Early-enhancing non-neoplastic lesions on gadolinium-enhanced MRI of the liver. Clin Radiol 58:778–786
50. Holland AE, Hecht EM, Hahn WY et al (2005) Importance of small (<20-mm) enhancing lesions seen only during the hepatic arterial phase at MR imaging of the cirrhotic liver: evaluation and comparison with whole explanted liver. Radiology 237:938–944
51. Caturelli E, Biasini E, Bartolucci F et al (2002) Diagnosis of hepatocellular carcinoma complicating liver cirrhosis: utility of repeat ultrasound-guided biopsy after unsuccessful first sampling. Cardiovasc Intervent Radiol 25:295–299
52. Scholmerich J, Schacherer D (2004) Diagnostic biopsy for hepatocellular carcinoma in cirrhosis: useful, necessary, dangerous, or academic sport? Gut 53:1224–1226
53. Kadoya M, Matsui O, Takashima T et al (1992) Hepatocellular carcinoma: correlation of MR imaging and histopathologic findings. Radiology 183:819–825
54. Earls J-P, Theise N-D, Winreb JB et al (1996) Dysplastic nodules and hepatocellular carcinoma: thin-section MR imaging of explanted livers with pathologic correlation. Radiology 201:207–214
55. Matsui O, Kadoya M, Kameyama T et al (1989) Adenomatous hyperplastic nodules in the cirrhotic liver: differentiation from hepatocellular carcinoma with MR imaging. Radiology 173:123–126
56. Edmondson HA, Steiner PE (1954) Primary carcinoma of the liver: a study of 199 cases among 48,900 necropsies. Cancer 7:462–503
57. Shinmura R, Matsui O, Kobayashi S et al (2005) Cirrhotic nodules: association between MR imaging signal intensity and intranodular blood supply. Radiology 237:512–519
58. Ebara M, Ohto M, Watanabe Y et al (1986) Diagnosis of small hepatocellular carcinoma: correlation of MR imaging and tumor histologic studies. Radiology 159:371–377
59. Kitagawa K, Matsui O, Kadoya M et al (1991) Hepatocellular carcinomas with excessive copper accumulation: CT and MR findings. Radiology 180:623–628
60. Kim CK, Lim JH, Park CK et al (2005) Neoangiogenesis and sinusoidal capillarization in hepatocellular carcinoma: correlation between dynamic CT and density of tumor microvessels. Radiology 237:529–534
61. Hayashi M, Matsui O, Ueda K et al (2002) Progression of hypervascular hepatocellular carcinoma: correlation with intranodular blood supply evaluated with CT during intraarterial injection of contrast material. Radiology 225:143–149
62. Tanaka O, Ito H, Yamada K et al (2005) Higher lesion conspicuity for SENSE dynamic MRI in detecting hypervascular hepatocellular carcinoma: analysis through the measurements of liver SNR and lesion - liver CNR comparison with conventional dynamic MRI. Eur Radiol 15:2427–2434

63. Nicolau C, Catala V, Vilana R et al (2004) Evaluation of hepatocelluar carcinoma using SonoVue, a second generation ultrasound contrast agent: correlation with cellular differentiation. Eur Radiol 14:1092–1099
64. Kudo M (2006) Early detection and characterization of hepatocellular carcinoma: value of imaging multistep human hepatocarcinogenesis. Intervirology 49:64–69
65. Efremidis SC, Hytiroglou P (2002) The multistep process of hepatocarcinogenesis in cirrhosis with imaging correlation. Eur Radiol 12:753–764
66. Ueda K, Matsui O, Kawamori Y et al (1998) Hypervascular hepatocellular carcinoma: evaluation of hemodynamics with dynamic CT during hepatic artreriography. Radiology 206:161–166
67. Wanless IR (2005) Liver biopsy in the diagnosis of hepatocellular carcinoma. Clin Liver Dis 9:281–285
68. Kojiro M (2004) Focus on dysplastic nodules and early hepatocellular carcinoma: an eastern point of view. Liver Transpl 10:S3–S8
69. Matsui O (2005) Detection and characterization of hepatocellular carcinoma by imaging. Clin Gastroenterol Hepatol 3(10 Suppl 2):S136–S140

Dig Dis Sci (2007) 52:1987–1994
DOI 10.1007/s10620-006-9146-9

ORIGINAL PAPER

Significance of Enhanced Expression of Nitric Oxide Syntheses in Splenic Sinus Lining Cells in Altered Portal Hemodynamics of Idiopathic Portal Hypertension

Yasunori Sato · Seiko Sawada · Kazuto Kozaka · Kenichi Harada · Motoko Sasaki · Osamu Matsui · Yasuni Nakanuma

Received: 5 July 2005 / Accepted: 10 November 2005 / Published online: 7 April 2007

Abstract Idiopathic portal hypertension (IPH) is characterized by noncirrhotic portal hypertension due mainly to increased intrahepatic, presinusoidal resistance to portal blood flow. Marked splenomegaly is always seen in IPH. To clarify the pathogenetic significance of splenomegaly, immunohistochemical expression of inducible nitric oxide synthese (iNOS), endothelial NOS (eNOS), and endothelin-1 (ET-1) in spleens from patients with IPH was examined. Sinus lining cells of IPH spleens showed diffuse and strong expression of iNOS and eNOS. Sinus lining cells of spleens from patients with liver cirrhosis (LC) also showed positive signals for iNOS and eNOS, but the staining intensity was significantly weak. ET-1 was detectable in only a few mononuclear leukocytes in the red pulp of both IPH and LC spleens. These results suggest that NO liberated in spleen, rather than ET-1, is responsible for the dilatation of splenic sinuses, leading to splenomegaly, and thereby contributes to portal hypertension in IPH.

Keywords Idiopathic portal hypertension · Spleen · Nitric oxide · Endothelin

Introduction

Idiopathic portal hypertension (IPH) is a condition with noncirrhotic portal hypertension of unknown etiology [1–3]. IPH is clinically characterized by marked splenomegaly with anemia or pancytopenia, esophageal varices, and variceal bleeding [4]. Liver function tests are mostly normal or mildly abnormal. Pathologically, portal phlebosclerosis, obliteration of intrahepatic small veins, and subcapsular parenchymal atrophy are characteristic of IPH liver [1, 2, 5, 6]. IPH is generally accepted as portal hypertensive disease due mainly to increased intrahepatic resistance, while increased portal venous blood flow into the liver also may contribute to its pathogenesis [1]. Although immunological abnormality or bacterial infection has been proposed as a possible etiopathogenesis of IPH [1, 7], the primary cause involved in the development of IPH remains unknown.

Portal hypertension directly causes passive congestion of the spleen. Portal venous flow into the liver in patients with hepatitis virus-related liver cirrhosis (LC) is reportedly comparable to that in normal persons. In IPH, however, splenic and portal venous blood flow are increased with dilatation of the portal vein trunk [1]. From the histopathological viewpoint, splenomegaly in IPH is characterized by proliferation of sinus endothelial cells and by irregulary widened interendothelial slits of the sinuses, and this feature of microvascular architecture of the red pulp of IPH spleen is reported to be different from that of LC [8]. Taken together, the cause and nature of splenomegaly in IPH seem to be different from those in LC.

In LC, it has been shown that the spleen is a source of several biologically active substances, and these substances secreted into portal blood may affect the process of liver regeneration in LC [9, 10]. Recently, a number of vasoactive substances have been implicated as potential mediators of portal hypertension. Among them, nitric oxide (NO) and endothelins (ETs) have received the greatest attention [11]. NO is a potent vasodilator, and there are three isoforms of NO synthese (NOS): inducible NOS (iNOS), endothelial

Y. Sato · S. Sawada · K. Harada · M. Sasaki · Y. Nakanuma (✉)
Department of Human Pathology, Kanazawa University Graduate School of Medicine, Kanazawa 920-8640, Japan
e-mail: pbcpsc@kenroku.kanazawa-u.ac.jp

K. Kozaka · O. Matsui
Department of Radiology, Kanazawa University Graduate School of Medicine, Kanazawa, Japan

NOS (eNOS), and neuronal NOS [12, 13]. ETs, however, are a family of three related peptides, designated ET-1, ET-2, and ET-3, that act as potent vasoconstrictors [14]. The respective roles of iNOS, eNOS, and ET-1 in intrahepatic vasoregulation have been well studied in cirrhotic liver [11].

Plasma concentrations of nitrite/nitrate (NOx; stable metabolites of NO) and ET-1 are elevated in cirrhotic patients. Recently, Nagasue *et al.* [15] identified the spleen as a major plasma source of ET-1 in cirrhotic patients. Plasma NOx and ET-1 levels are also elevated in IPH patients [16], suggesting that NO and ET-1 are involved in the altered hemodynamics of IPH. To date, however, the effect and participation of the spleen on the pathogenesis of IPH have not been well studied.

In this study, we investigated the expression of iNOS, eNOS, and ET-1 in the spleens of IPH using immunohistochemical technique and compared the results with those obtained from LC and controls without splenomegaly. The significance of the expression of these vasoactive substances in the altered hemodynamics of IPH is also discussed.

Materials and methods

Preparation of spleen specimens

Spleen specimens were obtained from 40 cases (IPH, $n = 10$; LC, $n = 10$; control, $n = 20$). Most of the spleens were obtained at autopsy (see below), which was performed during the period between 1989 and 2002 at Kanazawa University Graduate School of Medicine, Kanazawa, Japan. Surgically resected spleens obtained from Kanazawa University Hospital and affiliated hospitals were also included. Mean age, gender, and mean splenic weight of the three groups are summarized in Table 1. Other clinicopathological findings were, as follows.

IPH

Four surgically resected spleens and six autopsy materials were included. In all cases, the liver was histologically studied, compatible with the diagnosis of IPH. Esophageal varices were present in seven cases. In six autopsy cases, the livers were remarkably atrophic, with a mean liver weight of 696 g. Two cases had thromboembolism of large portal veins. There was no histological evidence of LC and no serological evidence of viral infection in 10 cases.

Table 1 Main features of the cases studied

	n	Sex (M:F)	Age (yr)	Splenic weight (g)
IPH	10	3:7	59 ± 19	473 ± 310
LC	10	4:6	67 ± 10	368 ± 142
Controls	20	13:7	68 ± 16	93 ± 43

Note. M, male; F, female; IPH, idiopathic portal hypertension; LC, liver cirrhosis.

LC

All were autopsy cases. The causes of LC were due to persistent hepatitis viral infection (hepatitis B, $n = 1$; hepatitis C, $n = 9$), and histological observation confirmed LC in all cases. Two cases had esophageal varices. In a single case, thromboembolism in a large portal vein was observed. All cases showed evident splenomegaly.

Controls

All were autopsy cases, which included patients who had gastric cancer, colon cancer, acute myocardial infarction, and cerebral hemorrhange. Findings of liver histology were nonspecific in all 20 cases, and splenomegaly was not evident

Patients who had infectious disease other than viral hepatitis, disorders of the hematopoietic and lymphoid systems, metabolic disorders, and autoimmune disease, which would affect the histology of the spleen, were excluded from this study. The study was conducted according to the provisions of the Declaration of Helsinki.

Immunohistochemistry

One to several regions were prepared from the spleen hilus. They were fixed in neutral formalin, and paraffin-enbedded tissue sections, 4 μm thick, were prepared. Sections were routinely stained with hematoxylin/eosin (HE) and periodic acid-Schiff (PAS), and other sections were subjected to the following immunohistochemical staining.

Immunohistochemistry was performed using an EnVision+ system (DAKO, Glostrup, Denmark) and primary antibodies against either iNOS (clone 54; mouse monoclonal; BD Biosciences, Franklin Lakes, NJ), eNOS (sc-654; rabbit polyclonal; Santa Cruz Biotechnology, Inc., Santa Cruz, CA), or ET-1 (clone TR.ET.48.5; mouse monoclonal; Affinity BioReagents, Inc., Golden, CO). After deparaffinization, antigen retrieval was performed by microwaving in 10 mM citrate buffer, pH 6.0, for 20 min for iNOS and eNOS staining and by incubation in 0.1% trypsin/phosphate-buffered saline (PBS) for 10 min at 37°C for ET-1 staining. To block the activity of endogenous peroxidase, sections were immersed in 0.3% hydrogen peroxidase in methanol for 20 min at room temperature. After pretreatment with blocking serum (DAKO), sections were incubated overnight at 4°C with individual primary antibodies: anti-iNOS (1:200), anti-eNOS (1:200), and anti-ET-1 (1:250). Then sections were incubated with secondary antibodies conjugated to peroxidase-labeled polymer, using the EnVision+ system.